GEOFLUIDS

Geofluids (2011) **11**, 34–47 doi: 10.1111/j.1468-8123.2010.00304.x

Geophysical and geochemical evidence of large scale fluid flow within shallow sediments in the eastern Gulf of Mexico, offshore Louisiana

A. GAY[1,2], Y. TAKANO[3,4], W. P. GILHOOLY III[5,6], C. BERNDT[1,7], K. HEESCHEN[1], N. SUZUKI[3], S. SAEGUSA[3], F. NAKAGAWA[3], U. TSUNOGAI[3], S. Y. JIANG[8] AND M. LOPEZ[2]

[1]Geology & Geophysics Research Group, National Oceanography Centre, Southampton, UK; [2]Laboratoire Géosciences Montpellier, University of Montpellier, Montpellier Cedex, France; [3]Department of Natural History Sciences, Graduate School of Science, Hokkaido University, Sapporo, Japan; [4]The Institute for Research on Earth Evolution (IFREE), Japan Agency for Marine-Earth Science & Technology (JAMSTEC), Yokosuka, Japan; [5]Department of Environmental Sciences, University of Virginia, Charlottesville, VA, USA; [6]Department of Earth Sciences, University of California, Riverside, CA, USA; [7]IFM-GEOMAR, Leibniz Institute for Marine Sciences, Kiel, Germany; [8]State Key Laboratory for Mineral Deposits Research and Center for Marine Geochemistry Research, Nanjing University, Nanjiing, China

ABSTRACT

We analyse the fluid flow regime within sediments on the Eastern levee of the modern Mississippi Canyon using 3D seismic data and downhole logging data acquired at Sites U1322 and U1324 during the 2005 Integrated Ocean Drilling Program (IODP) Expedition 308 in the Gulf of Mexico. Sulphate and methane concentrations in pore water show that sulphate–methane transition zone, at 74 and 94 m below seafloor, are amongst the deepest ever found in a sedimentary basin. This is in part due to a basinward fluid flow in a buried turbiditic channel (Blue Unit, 1000 mbsf), which separates sedimentary compartments located below and above this unit, preventing normal upward methane flux to the seafloor. Overpressure in the lower compartment leads to episodic and focused fluid migration through deep conduits that bypass the upper compartment, forming mud volcanoes at the seabed. This may also favour seawater circulation and we interpret the deep sulphate–methane transition zones as a result of high downward sulphate fluxes coming from seawater that are about 5–10 times above those measured in other basins. The results show that geochemical reactions within shallow sediments are dominated by seawater downwelling in the Mars-Ursa basin, compared to other basins in which the upward fluid flux is controlling methane-related reactions. This has implications for the occurrence of gas hydrates in the subsurface and is evidence of the active connection between buried sediments and the water column.

Key words: focused fluid flow, SMT, seal bypass system, pockmark, mud volcano, overpressure, pipe, 3D seismic, IODP Expedition 308, Gulf of Mexico

Received 9 October 2009; accepted 1 July 2010

Corresponding author: Aurélien Gay, Géosciences Montpellier, Université Montpellier 2, 34095 Montpellier Cedex, France.
Email: aurelien.gay@gm.univ-montp2.fr. Tel: +33 (0) 4 67144598. Fax: +33 (0) 4 67143908.

Geofluids (2011) **11**, 34–47

INTRODUCTION

Gas venting along passive continental margins is a widespread phenomenon (Berndt 2005). However, our knowledge about the driving processes is limited to the few deep datasets available. Fluids migrate along different pathways and their seepage is usually expressed as seafloor features such as pockmarks or mud volcanoes (Loncke *et al.* 2004; Zitter *et al.* 2005; Gay *et al.* 2007). Even if differential buoyancy naturally drives fluid upward, focused fluid migration is generally triggered by the interaction of several processes including: (i) pore fluid overpressure: sand-rich deepwater channels embedded within fine-grained sealing layers can preserve porosity and delay lithification, which favours liquefaction and upward fluid migration (Osborne & Swarbrick 1997); (ii) overpressure in sand-rich reservoirs

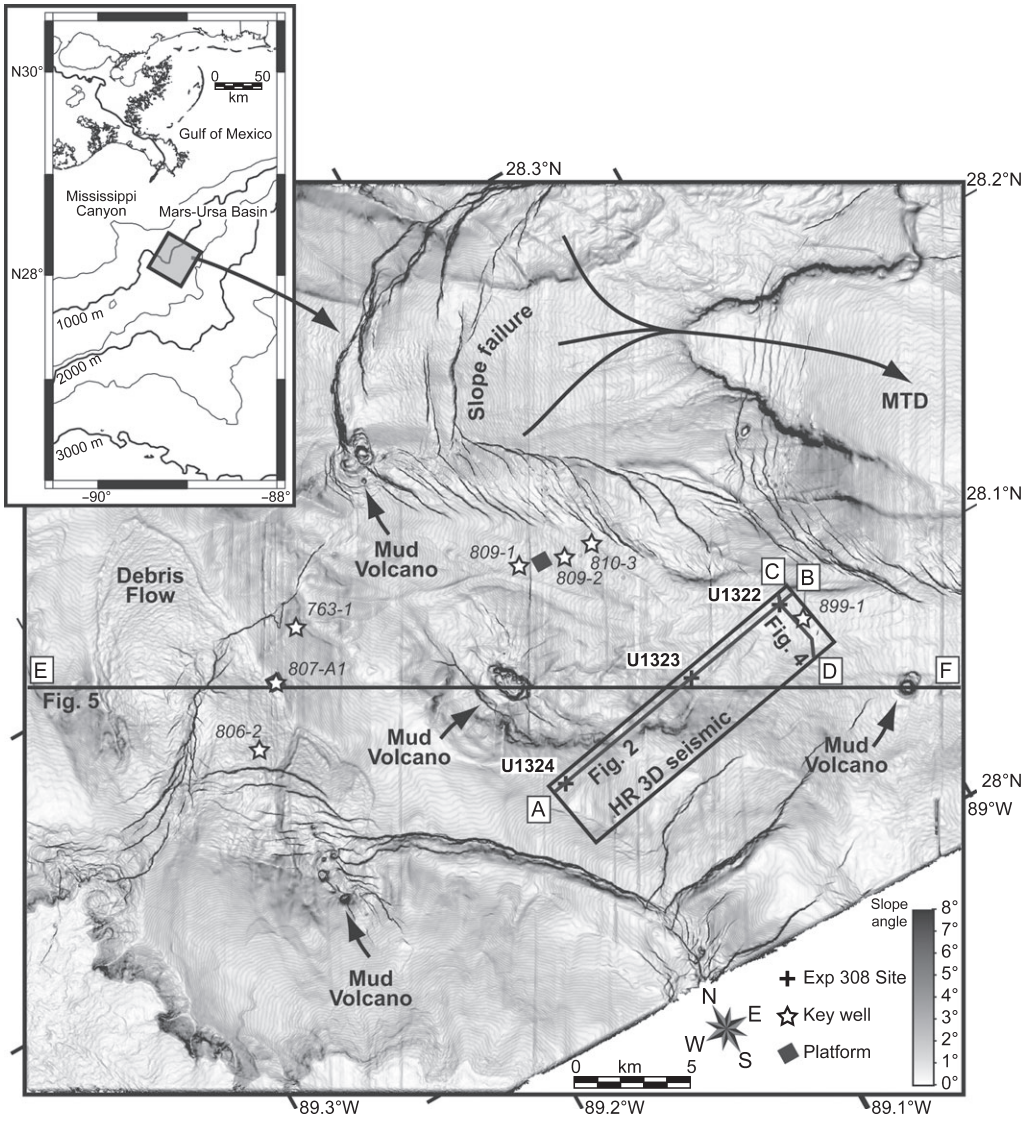

Fig. 1. Dip map of seafloor, on the eastern levee of the modern Mississippi canyon between 800 and 1400 m water depth, calculated from conventional (12.5 × 12.5 m) 3D seismic data. The seafloor is intensively remodelled by slope failures, debris flows, faulting and mud volcanoes. The empty black rectangle indicates the very high resolution (6.25 × 6.25 m) 3D seismic block used in this study. The three sites drilled during IODP Expedition 308, indicated by black crosses, are located at various positions along the slope and within the very high resolution 3D seismic area, allowing accurate correlation between both datasets. Petroleum drilling sites, indicated by stars, allowed correlation across the basin.

affected by hydrocarbon charges (Yu & Lerche 1996); (iii) earthquakes; (iv) differential compaction and folding across thick sand bodies, which may generate upward propagating fractures at the edges, and downward propagating cracks over crests (Cosgrove & Hillier 2000); (v) lateral transfert of pressure (Osborne & Swarbrick 1997).

The Mars-Ursa Basin (Fig. 1) on the eastern levee of the modern Mississippi Canyon, at 800–2000 m water depth is a particularly suitable site to study the processes that control fluid expulsion, because of the comprehensive data set that exists for this basin. It includes conventional and high resolution 3D seismic data provided by Shell and downhole logs and geochemical data acquired during the Integrated Ocean Drilling Program (IODP) Expedition 308.

The objective of this article is to understand the effects of a stratal fluid pathway, namely the Blue Unit on the fluid migration pattern in the overlying sediments. To reach this objective, we first analyse the geochemical and geophysical evidence for each of the IODP sites and integrate it with the seismic data to establish the different sources for the fluids that are migrating through the surface sediments. In a second step, we deduce a geological fluid plumbing system that explains the geochemical anomalies and is consistent with the seismic observations.

GEOLOGICAL SETTING

Integrated Ocean Drilling Program Expedition 308 sampled sediments in the vicinity of the Mississippi Canyon (Flemings *et al.* 2005; Behrmann *et al.* 2006). The Mars-Ursa basin resulted from the interplay between sedimentation and erosion during the late Pleistocene, beginning about 70 ka BP (McFarlan & LeRoy 1988). In response to the late Wisconsinan glaciation during marine isotope stages 2–4 (Winker & Booth 2000; Winker & Shipp 2002), sea level fall has led to rapid deposition of thick sand and mud sequences (Coleman & Roberts 1988) referred to as the 'Blue Unit' (Sawyer *et al.* 2007), which is interpreted as a stacked turbidite deposit. On seismic profile AB (Fig. 2), the base (Base Blue) and the top (S80) of the Blue Unit correspond to continuous high amplitude reflections and can be mapped from west to east throughout the study area. The thickness of the Blue Unit increases towards the east, where the top of the unit rises to within 250 ms two-way traveltime (TWT) (approximately 200 m) below seafloor (Sawyer *et al.* 2007).

Whereas the Pass and Ursa Canyons eroded and incised the Blue Unit further north (Pulham 1993), levees of these canyons are overlying the Blue Unit in the studied area. These levees consist of a succession of slope failures identified both on the seismic profile AB and within the recovered cores (Fig. 2). Oil industry wells (899-1, 810-3, 809-1, 809-2, 763-1) show that the Blue Unit consists of several 1–7 m thick sand beds that are separated by approximately 5 m thick mud layers (Sawyer *et al.* 2007).

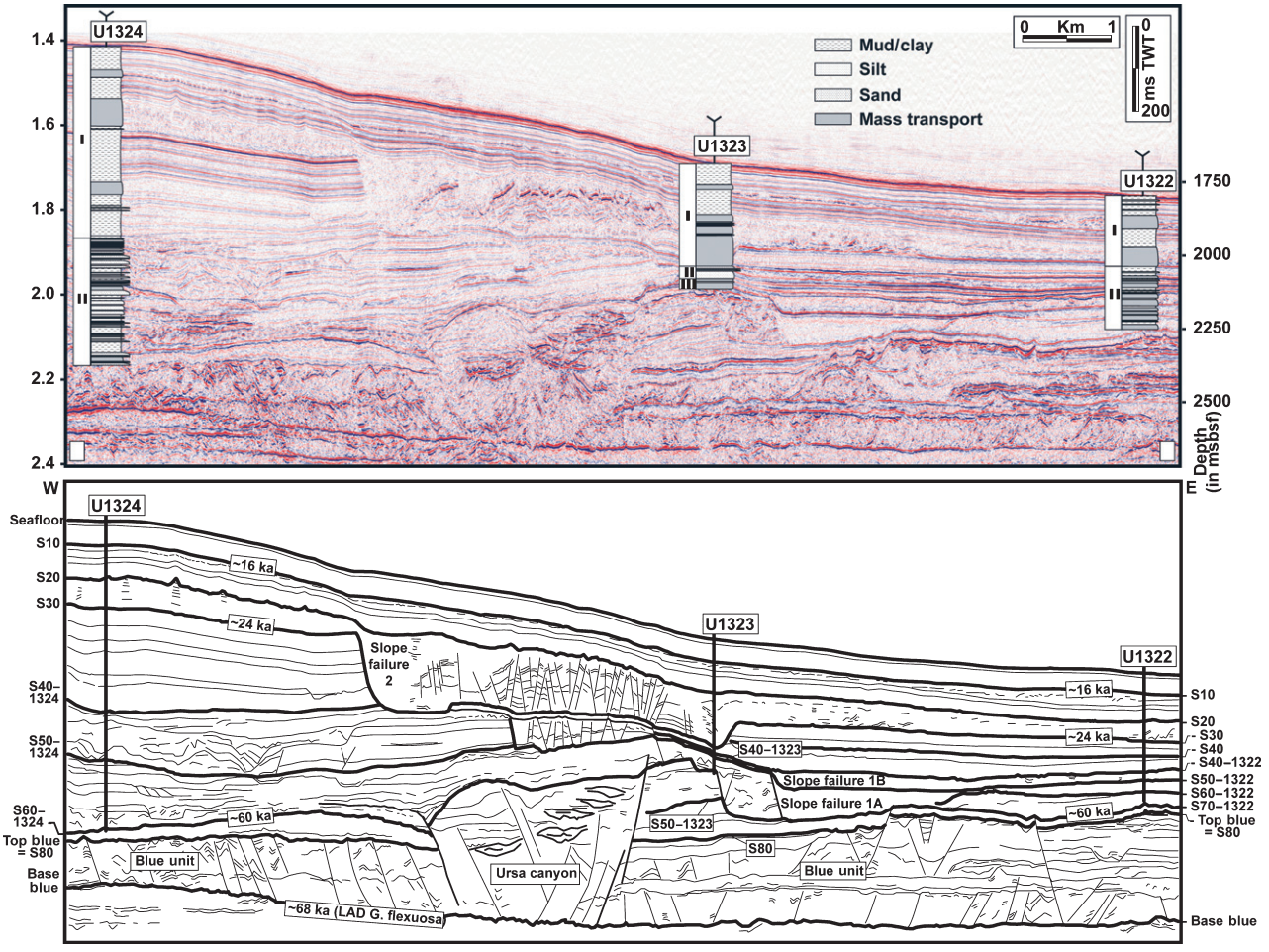

Fig. 2. Top: Seismic profile AB, from very high resolution 3D seismic data, crossing the three IODP Expedition 308 drilled sites from West to East. The upper interval over the Blue Unit was fully penetrated by IODP wells and interpreted logs from Site U1322 to Site U1324 are reported here. At both sites U1324 and U1322, this sequence is composed of a succession of silt and sand layers, to 10 m thick, and mass transport deposits, interbedded with mud. The mass transport deposits are the result of failures slope on the levees of Pass and Ursa Canyons. The log at site U1323 is derived from a geotechnical hole. Bottom: Line drawing showing the stratigraphic interpretation of the seismic line based on seismic stratigraphy and well interpretation. Some reflections can be correlated from well to well (S10–S40) but, because of the large number of mass transport deposits that developed on the levees of the Mississippi canyon, most of them have been labelled relating to the well vicinity (i.e. S50-1322 for the horizon at Site U1322).

The sequence overlying the Blue Unit was fully penetrated by IODP wells U1322 and U1324. Site U1324 is composed of a sequence of silt and sand layers, up to 10 m thick, interbedded with mud. Some thick sand layers have been correlated to continuous high amplitude reflections on seismic profile AB (S60-1324, S50-1324). Site U1322 is composed of a succession of mass transport deposits, which are the result of slope failures on the levees of Pass and Ursa Canyons. The bases of the mass transport deposits intervals are clearly seen on the seismic profile AB (S40, S40-1322, S50-1322 and S60-1322). Their chaotic seismic character makes the correlation between wells particularly difficult, but the top of the sequence is marked by the continuous horizon S40. Above this feature, high amplitude continuous reflections (S10, S20 and S30) clearly correlate between wells. The uppermost unit is a hemipelagic drape which is intensively remodelled by various processes, including debris flows, slope failures, faulting, fluid expulsion and mud volcanism. The most recent slope failure, visible on the modern seafloor (see Fig. 1), is described as one of the largest submarine mass transport deposits in the world (McAdoo *et al.* 2000). The Louisiana continental slope is a dynamic basin with deposition rates that exceed 2 km Myr^{-1} in some areas. This high sedimentation rate is of primary importance in overpressure generation leading to fluid expulsion (Yu & Lerche 1996). In the Mars-Ursa basin total sediment thickness is in excess of 16 km.

SAMPLING AND METHODS

In situ pressure and temperature were measured with the temperature to pressure (T2P) and the Davis-Villinger temperature–pressure probe (Flemings *et al.* 2005). These downhole tools are designed to make rapid measurements in low-permeability sediments. Temperature measurements were also made during coring using the advanced piston corer temperature tool.

Whole-round sections were cut from the core immediately after recovery on deck. The surfaces of the samples were scraped with a Teflon-coated spatula to remove sediment potentially contaminated with drilling fluids and each sample was squeezed by applying to 40 000 lb of pressure in a titanium squeezer. Interstitial water was extracted directly into a 60-ml plastic syringe and sample splits were filtered through a 0.45-μm acrodisc filter. Sulphate concentrations were determined on a DionexDX100 ion chromatograph and calibrated using IAPSO standards (Gieskes *et al.* 1991).

Hydrocarbons were analysed on board *JOIDES Resolution* according to the headspace sampling method developed for IODP (Pimmel & Claypool 2001). A 5-cm^3 sediment sample was collected every 10 m, sealed in a preashed glass serum vial, and heated at 70°C for 20 min. The evolved C_1 through C_3 hydrocarbons (methane, ethane and propane) were drawn from the headspace, injected on a Hewlett Packard 5890 gas chromatograph, and quantified with a flame ionization detector.

Shore-based analysis of the concentration and stable carbon isotopic composition of methane and ethane was conducted using gas chromatography-combustion-isotope ratio mass spectrometry (Tsunogai *et al.* 1999). A magnesium perchlorate/Ascarite trap removed H_2O and CO_2 impurities prior to cryogenic purification (−183°C) and separation of methane from other gases by mini-GC (10 mm Porapak-Q column). High purity methane was then injected into the head of a PoraPLOT-Q capillary column at liquid oxygen temperature (−183°C) to concentrate methane at the head of the separation column. The column head was then rapidly heated to 80°C under a continuous helium flow of 3.0 ml min^{-1}. The column-separated methane was then oxidized to CO_2 in a 960°C combustion furnace (CuO/Pt catalyst) and introduced into a Finnigan MAT 252 mass spectrometer to determine $^{13}C/^{12}C$ ratios. The relative error in the determination of the concentration was <3%. The overall precision of $\delta^{13}C$ analysis was ±0.2‰.

The seismic data used for this study were extracted from high and very high resolution 3D seismic surveys of shallow water drilling hazards in the area (see Fig. 1). The conventional 3D-data selected for this study covers an area of about 1600 km^2 with an in-line and cross-line spacing of 12.5 m and a sampling rate of 4 ms TWT. The very high resolution 3D seismic block covers an area of about 35 km^2 with an in-line and a cross-line spacing of 6.25 m and a sampling rate of 1 ms TWT. The data were loaded and interpreted with SHELL's inhouse seismic interpretation software.

PHYSICAL PROPERTIES AND GEOCHEMICAL ANALYSIS

Site U1324

Site U1324 is characterized by a thick sedimentary cover (612 m) above the Blue Unit (Fig. 3). Gamma radiation and resistivity increase rapidly from the mudline down to 20 mbsf and then gradually increase with little small scale variability down to the base of Unit I at 362 mbsf. This profile corresponds to the hemipelagic drape composed of thick mud and clay intervals interlayered with some mass transport deposits. At greater depth, in Unit II, logging data show a high variability, partly due to poor borehole conditions, with peaks correlated to silt and sand intervals (Fig. 3). The Logging While Drilling resistivity images show evidence of deformation, such as folds, variable dips, tilted beds and faults.

Porosity as measured by the moisture and density method decreases from 78% at the seafloor to 50% at the base of Lithostratigraphic Unit I (Fig. 3). Porosity is lower

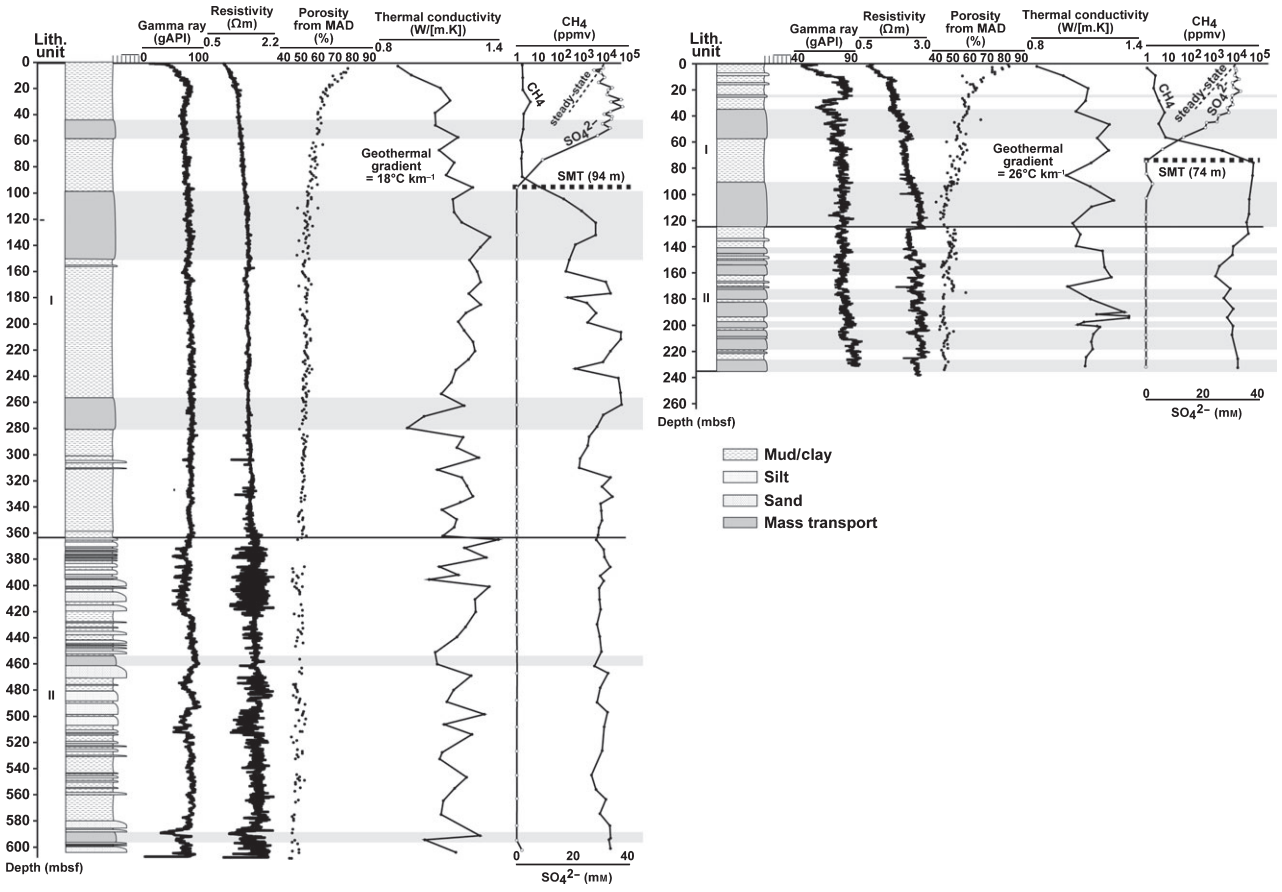

Fig. 3. Left: Physical properties, including Gamma Ray, Resistivity, porosity (from MAD), thermal conductivity (see text for more details), and methane and sulphate profiles at Site U1324. The decrease of SO_4^{2-} contents to below detection (2.89 mM) at 94 mbsf determines the depth of the sulphate–methane transition zone. The first tens of metres below the seafloor are characterized by high sulphate content, close or higher than seawater (28.9 mM). The dashed line represents the sulphate profile for steady-state conditions. Right: Physical properties, including Gamma Ray, Resistivity, porosity (from MAD), thermal conductivity (see text for more details), and methane and sulphate profiles at Site U1322. The decrease of SO_4^{2-} contents to below detection (2.89 mM) at 74 mbsf determines the depth of the sulphate–methane transition zone. The first tens of metres below the seafloor are characterized by high sulphate content, close or higher than seawater (28.9 mM). The dashed line represents the sulphate profile for steady-state conditions.

in the mass transport deposits than in mud or silt layers indicating that they are denser than their bounding sediments (Flemings *et al.* 2005). In Lithostratigraphic unit II, porosity is higher in silt and sand than in mud layers.

Thermal conductivities lie between 0.85 W mK^{-1} at the seafloor and 1.1 W mK^{-1} at the base of Lithostratigraphic Unit I (Fig. 3). At the transition between the upper and the lower unit, the stepwise increase in thermal conductivity to 1.4 W mK^{-1} at the transition between the upper and the lower unit becomes highly variable to the base of the borehole. Temperature measurements indicate a geothermal gradient of 18°C km^{-1} (Flemings *et al.* 2005).

Methane concentrations are very low (close to the detection limit: 10 ppmv) from the seafloor to 90 mbsf but exhibit a five-fold increase below this depth (Fig. 3). Maximum methane concentrations occur between 212 mbsf (40339 ppmv) and 261 mbsf (41620 ppmv) and remain high throughout Unit I. The methane content is variable in this interval, and methane peaks are found below mass transport deposits. Methane concentrations in Unit II remain high to the base of the borehole, but are less variable and do not depend on lithology. Methane is the predominant hydrocarbon with traces of ethane (<3.5 ppmv) and ethylene (<1.5 ppmv) in a few samples.

The sulphate profile shows a slight increase from 30.6 mM just below the seafloor (28 mM in seawater) to a maximum of 37.3 mM at 35 mbsf (Fig. 3). A distinct concentration gradient is observed between 55 and 94 mbsf. At that depth the sulphate concentration tends to 0 (detection limit of 2.89 mM) and corresponds to the depth at which methane concentration starts to increase.

The C_1/C_2 ratios at Site U1324 are >6000, suggesting a biogenic origin of hydrocarbons (Whiticar 1999). This interpretation is supported by the light isotopic signature of methane ($\delta^{13}C$ = −81.7‰ to −86.7‰) and ethane ($\delta^{13}C$ = −44.1‰ to −46.8‰) (Table 1).

Table 1 Isotopic composition of methane and ethane from headspace gases sampling at site U1324 and U1322.

mbsf	$\delta^{13}C$ Methane (in ‰)	$\delta^{13}C$ Ethane (in ‰)
U1324		
278.1	−85.3	−44.1
293.4	−81.7	−44.2
302.4	−85.5	−44.6
332.1	−86.7	−45.8
349.5	−85.9	−45.6
355.6	−84.9	−46.8
385.9	−82.5	−45.5
U1322		
120.8	−86.5	−37.6
138.8	−81.4	−39.3
186.8	−61.6	−45.9
207.1	−69.0	−48.7
224.8	−74.7	n.d.

Site U1322

Drilling at Site U1322 was terminated above the top of the Blue Unit at 234.5 mbsf. This deep water site penetrated thinner sedimentary cover over the permeable Blue Unit relative to Site U1324. Gamma ray and resistivity measurements increase from seabed to 20 mbsf, trending towards higher values with depth (Fig. 3). The logging data mostly indicate a succession of clay, mud and occasionally silt that correlates to the lithostratigraphic descriptions.

Porosity as measured by the moisture and density method decreases rapidly from about 82% at the seafloor to 40% at the bottom of the hole. Again, porosity is lower in mass transport deposits than in mud or silt indicating a denser lithology.

Thermal conductivities lie between 0.8 W mK^{-1} at the seafloor and 1.1 W mK^{-1} at the bottom of the hole. Peak values of to 1.4 W mK^{-1} were observed in mass transport deposits (Fig. 3), again suggesting denser sediments in these intervals. Temperature measurements indicate a geothermal gradient of 26°C km^{-1}.

The methane concentration at Site U1322 is lower than the detection limit (10 ppmv) from the seafloor to 60 mbsf (Fig. 3). Between 60 and 74 mbsf, the methane gradient is very strong and methane reaches its maximum value of 51001 ppmv. The highest methane concentrations range between 51001 ppmv at 74 mbsf and 29536 ppmv at 129 mbsf. According to the lithological description, this gas-bearing interval consists of mass transport deposits interbedded with mud and clay. These strata also correlate with a slight increase of ethane. However, only traces of ethane (<3.4 ppmv) and ethylene (<2.6 ppmv) were detected.

The sulphate profile shows an increase from 31.4 mM at the seafloor (28 mM in seawater) to a maximum of 33.1 mM at 20.9 mbsf and then a decrease close to the detection limit of 2.89 mM at 74 mbsf (Fig. 3). The depth of the sulphate–methane transition zone is located at 74 mbsf at Site U1322.

The C_1/C_2 ratios at Site U1322 are generally higher than 9000, again suggesting a microbial origin of hydrocarbons (Whiticar 1999). Methane is isotopically depleted near the surface ($\delta^{13}C$ = −81.4‰ and −86.5‰ at 120.8 mbsf and 138.8 mbsf respectively), and becomes slightly heavier with depth ($\delta^{13}C$ = −61.6‰, −69‰ and −74.7‰ at 186.8 mbsf, 207.1 mbsf and 224.8 mbsf respectively). This shift in $\delta^{13}C$ may indicate a slight addition of thermogenic fluids. However, the $\delta^{13}C$ of ethane lies between −44.1‰ and −46.8‰, corresponding to a dominantly microbial signature from the seafloor to the bottom of the hole (Table 1).

GEOPHYSICAL EVIDENCE OF FOCUSED FLUID FLOW

The effects of subsurface fluid migration on oil and gas reservoirs, surface sediment processes, the water column and the atmosphere, have been the subject of many studies in the Gulf of Mexico (Brooks *et al.* 1984; MacDonald *et al.* 1993, 2002; Sassen *et al.* 1994; Fu & Aharon 1998; Cathles 2004). Compared to most of the Gulf of Mexico slope, the Mars-Ursa Basin is characterized by a relatively larger number of high-flux gas seeps through mud volcanoes (Sassen *et al.* 2003a,b), which indicates more efficient fluid focusing at depth (Milkov & Sassen 2000).

Fluid flow from the Blue Unit

In the eastern part of the area, the composite seismic profile CD crosses two pockmarks in a north-south direction (Fig. 4). Most of the pockmarks identified in the area are characterized by increased amplitudes and reversed polarities compared to the surrounding seabed (Fig. 4). This may be due to gas hydrates and/or carbonate builds-up or this is a pull-up effect of reflections because of the presence of gas within sediments. However, due to the absence of gas hydrates at the seabed in the area, reversal is most probably due to a poorly migrated image of a pockmark with a depressed base. This also suggests that fluid expulsion is still active or has been active until recently, as this evidence for fluid expulsion is not obscured by later sedimentation.

Almost all observed pockmarks are linked with underlying seismic pipes. Pipes are usually expressed as piercing structures, intensively remodelling surrounding sediments. They are interpreted to be the expression of highly focused migration of fluids through low permeability sediments (Løseth *et al.* 2001). They are characterized by a vertical columnar zone of seismic disturbance. The pipes are crudely cylindrical, but occasionally have steep conical geometry either narrowing upwards or downwards.

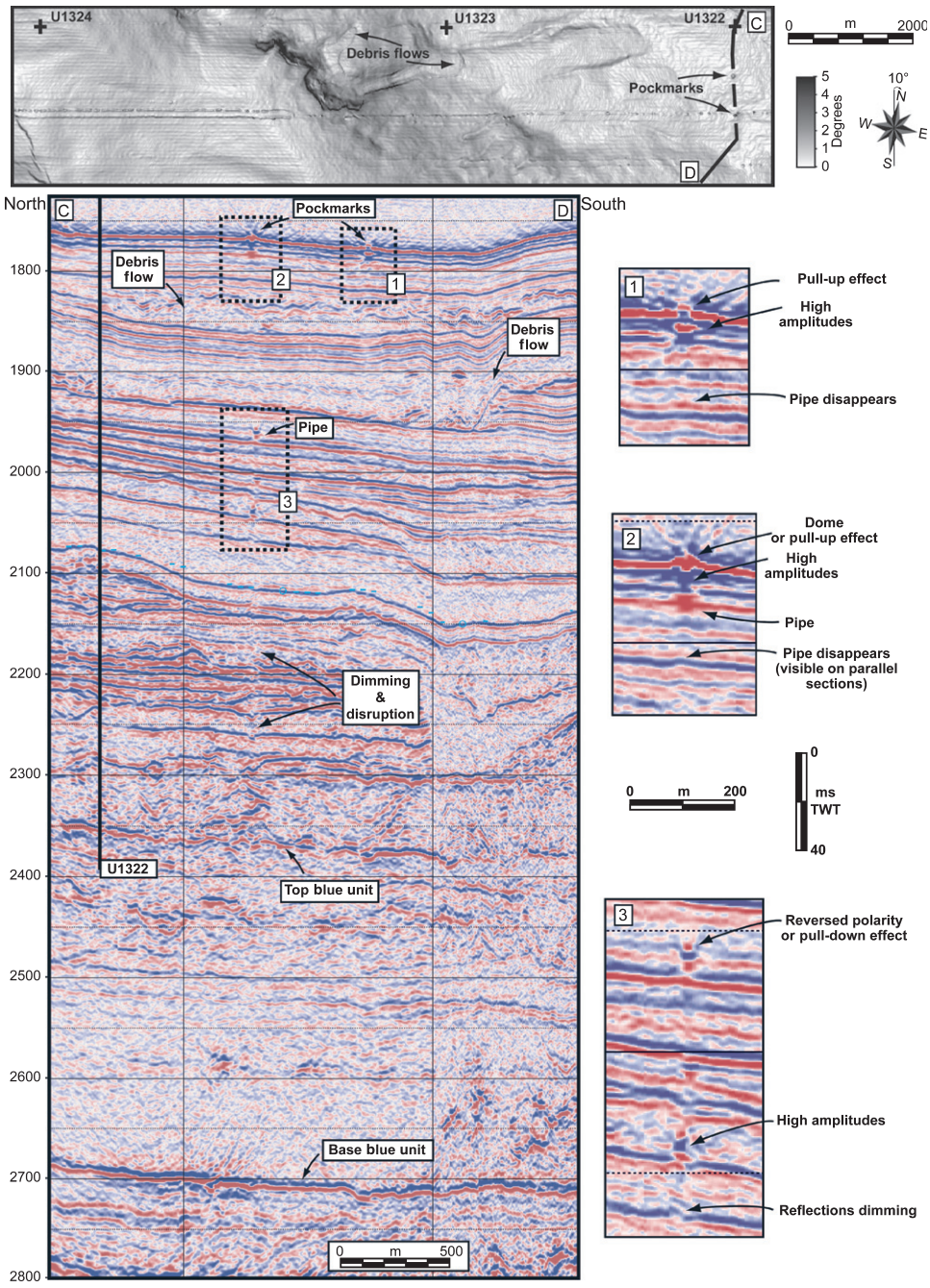

Fig. 4. Top: Dip map of seafloor from high resolution (6.25 × 6.25 m) 3D seismic data. Pockmarks are only identified on these high resolution data, and not on conventional 3D seismic data. Bottom: Seismic profile CD (see Fig. 1 for location), extracted from high resolution (6.25 × 6.25 m) 3D seismic data, crossing a pockmark and its related underlying pipe (see zoomed in views 1–3 for details). Even if its identification is tenuous, the pipe seems to penetrate the Blue Unit. Most of the pipes in the area source from the Blue Unit or from shallower depths, but most of the pockmarks are concentrated at the toe of the slope, close to Site U1322 and to the key-well 899-1. They have been formed during exploration drilling operations prior to IODP Expedition 308 drilling, and Shell's personal communication).

The descriptive base for pipe structures is generally based on geometrical-acoustic approach (Moss & Cartwright in press). The seismic profile CD clearly shows that pipes connect to the Blue Unit or originate from shallower strata (Fig. 4). The lack of any deeper seismic anomaly clearly indicates that fluids feeding pockmarks and pipes originate from this sand-rich level, as previously shown in West Africa (Gay *et al.* 2006). However, the small number of pockmarks and pipes and their small size (they are not visible in the conventional 3D seismic data) suggest that the

Blue Unit expelled very small amounts of fluids through focused conduits.

Fluid flow from below the Blue Unit

In the area covered by conventional 3D seismic data, we identified 12 mud volcanoes, typically 1–3 km wide, that are associated with fracture zones and slope failures (see Fig. 1). The biggest mud volcano, in terms of volume of remobilized sediments, sits 4 km north of IODP Site U1324. This mud volcano, imaged on seismic profile EF (Fig. 5), is about 2 km wide and rises 40–50 m above the seafloor. It is connected to an underlying vertical acoustic anomaly that is as large as the mud volcano itself and characterized by a dimming of reflections. This anomaly masks the feeding conduit for mud and fluid that is hard to interpret. On both sides of the acoustic anomaly, reflections are distorted and shifted upward. This signature is typical for mud volcanoes and diapirs and is probably caused by structural deformation during the ascent of mud through the overlying sediments (Kopf 2002; Davies & Stewart 2005; Stewart & Davies 2006). Relatively low seismic velocities, evidenced by pull-up effects in the disturbed zone, suggest that the conduit is filled with gas-charged sediments. The disturbed seismic reflections are observed as deep as 3000 ms TWT, suggesting that the source of mud and fluids is located deeper than the Blue Unit. Two other similar structures are visible on this profile (Fig. 5): a piercing mud volcano is visible on the western part and on the eastern part a smaller mud volcano is associated with an underlying narrow acoustic chimney, about 500 m wide. The acoustic anomaly displays a more complex structure in the upper 250 ms TWT below seafloor. However, at about 200 ms TWT below the seafloor, a dome structure is preserved over the S30 stratigraphic level. On both flanks of the dome, slides are clearly visible and the mound is therefore interpreted as a palaeo-mud volcano (Van Rensbergen *et al.* 1999).

DISCUSSION

Cause of lateral fluid flow in the Blue Unit

A study conducted on the New Jersey continental margin (Dugan & Flemings 2002) showed that pressure and stress profiles in an overpressured basin can be created solely by differential loading and variations in rock properties and do not require any other mechanism to lower the permeability

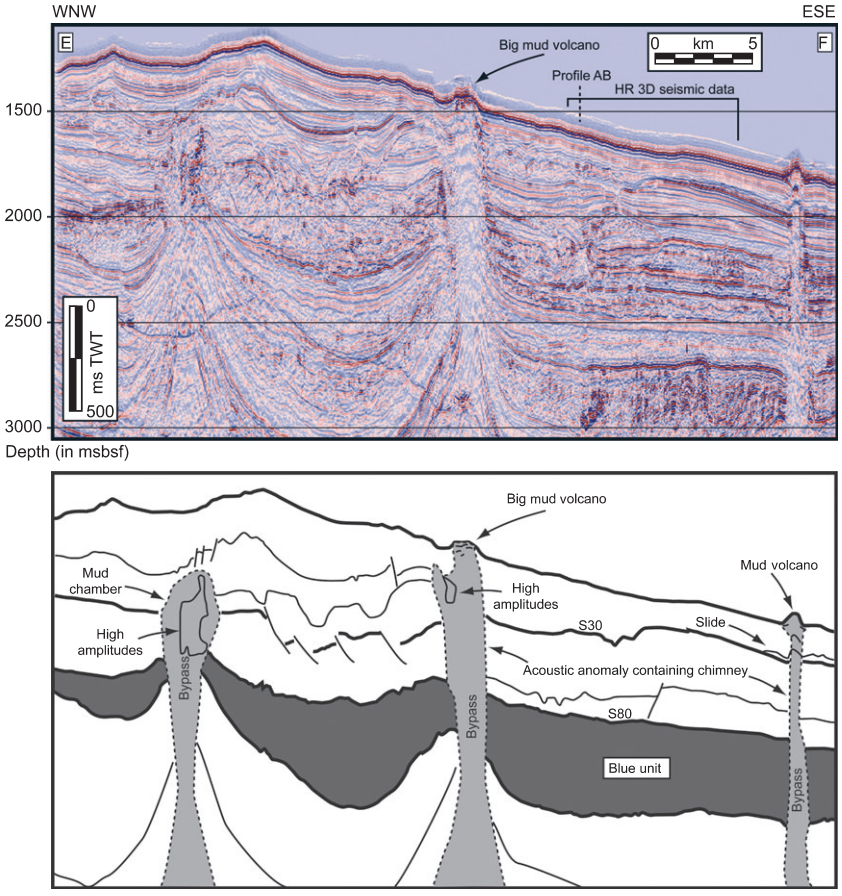

Fig. 5. Seismic profile EF (see Fig. 1 for location), extracted from conventional (12.5 × 12.5 m) 3D seismic data, showing mud volcanoes and piercing mud structures. The underlying conduits are as large as the mud volcanoes themselves, ranging from 500 to 2000 m in diameter. All mud volcanoes identified in the study area have a conduit that penetrates deeper than the Blue Unit, suggesting that the fluid overpressure from below the Blue Unit is released through these conduits and bypass the upper sequence over the Blue Unit.

and increase overpressure. Their model predicts that rapid loading produces high pressures near the depocenter, inducing a lateral transfer of pressure in permeable intervals. The lateral transfer of pressure would be much more effective in the case of a permeable aquifer extending hundreds of kilometres across the continental slope to create artesian conditions.

In the northern Gulf of Mexico, the Blue Unit is a thick accumulation of sand and mud considered to be an aquifer (Sawyer *et al.* 2007). It was rapidly and asymmetrically buried by thick, mud-rich levees of two deepwater systems. Both systems plunged from north to south with a steeper gradient than the underlying Blue Unit (Sawyer *et al.* 2007). The conditions of hydraulic connectivity are reached in the Mars-Ursa Basin where the differential loading over a permeable aquifer (Blue Unit) is the only requirement for producing a basinward fluid flow that transfers pressure from the shelf to the toe of the slope (Flemings *et al.* 2005).

In the Mars-Ursa Basin, pressure predictions based on porosity measurements show overpressures with a normalized (difference between measured pressure and lithostatic pressure) overpressure ratio $\lambda^* > 0.6$ (Fig. 6). Direct pressure measurements also record overpressures with $\lambda^* > 0.5$. At equivalent depths, pressures are slightly greater to the east at Site U1322, where the overburden is thinner than to the west at Site U1324. On average, sedimentation rates at Site U1324 were almost three times greater than at Site U1322 (10 mm year^{-1} versus 3.8 mm year^{-1}) (Flemings *et al.* 2005). The age model suggests that the sedimentation rate at the base of Site U1324 exceeded 25 and 16 m ka^{-1} at Site U1322 (Fig. 6). These observations show that the flow rate within sediments overlying the Blue Unit is similar at both sites, reflecting a constant overpressure gradient. A lateral flow within the Blue Unit is required to maintain the overpressure gradient at the two locations, despite the threefold difference in sedimentation rate.

The differential loading over the Blue Unit leads to a pressure gradient (Flemings *et al.* 2005; Urgeles *et al.* 2007) and a basinward fluid flow along sand-rich beds (Fig. 6), as the hydraulic connectivity is reached within the Blue Unit from Site U1324 to Site U1322 (Sawyer *et al.* 2007).

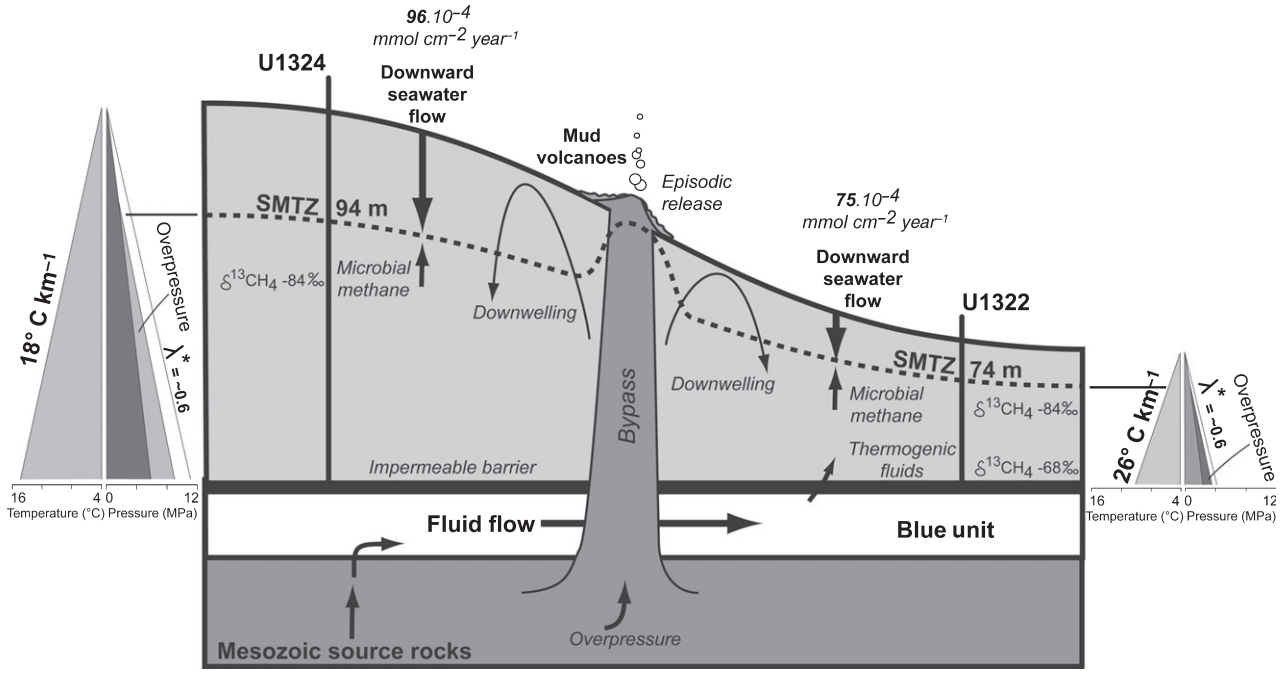

Fig. 6. Synthesis of the fluid flow regime within shallow (<1000 m) sediments above and below an overpressured deepwater channel. The basinward fluid flow gradient into the sand-rich channel, playing the role of an aquifer, is induced by the differential loading above it. This fluid flow gradient represents an impermeable barrier, and deep fluids coming from underlying Mesozoic source rocks and reservoirs are diverted into the lateral flow, disconnecting sedimentary compartments located below and above the aquifer. This is confirmed by: (i) the respective methane isotopic values at Site U1324 ($\delta^{13}C = -81.7‰$ to $-86.7‰$ PDB, average = $-84‰$) and Site U1322 ($\delta^{13}C = -81.4‰$ to $-86.5‰$ PDB, average = $-84‰$) showing that deep-derived thermogenic fluids are not circulating in the upper compartment, except a slight contribution at the toe of the slope near the bottom of hole U1322 ($\delta^{13}C = -61.6‰$ to $-74.7‰$ PDB, average = $-68‰$), and (ii) low geothermal gradients (18 and 26°C km^{-1}) measured in the upper compartment. Sulphate–methane transition zones have been determined from methane and sulphate profiles. It is amongst the deepest (74 and 94 m at Sites U1322 and U1324 respectively) ever found in deep basins. Due to a constant upward fluid (and thus methane) flow calculated from *in situ* pressure measurements, the depth of the sulphate–methane transition zone is mainly caused by a possible downward seawater flow into shallow sediments, as evidenced by elevated sulphate concentration and a high downward sulphate flux, 75 and 96×10^{-4} mmol cm^{-2} year^{-1} at Sites U1322 and U1324 respectively. Thermogenic fluids have been evidenced on several mud volcanoes of the Louisiana continental shelf, showing that deep fluids can reach the seafloor by bypassing the Blue Unit and the upper compartment.

Evidence of seal and diverted fluid flow

The isotopically depleted signature of the shallow gas measured at Sites U1322 and U1324 indicates local production of microbial methane that is isotopically distinct from thermogenic gases derived from depth. The light carbon isotope ratio of methane sampled from above the Blue Unit indicates negligible contribution of deep seated fluids into the overlying sediments, with the exception of a slight admixture of isotopically heavy thermogenic methane at the toe of the slope near the bottom of hole U1322 ($\delta^{13}C = -61.6‰$ to $-74.7‰$). The predominantly microbial methane signal suggests minimal mixing between microbial and thermogenic sources. This also suggests that venting of the thermogenic fluids generated in or below the Blue Unit remains confined to the cross-cutting conduits. The numerous mud volcanoes within the study area originate from the Blue Unit and provide obvious pathways for fluid escape to the seafloor (Fig. 6). Previous investigations conducted on mud volcanoes, north and south of the study area, reported shallow occurrences of thermogenic gas hydrates and carbonates, and biodegraded crude oil (Sassen *et al.* 1999, 2003a). Such venting features are also known to produce a substantial oil and gas flux into the overlying water column as shown by huge oil slicks detected from space (MacDonald *et al.* 1993).

The low carbon isotope values clearly demonstrate that the basinward fluid flow within the overpressured Blue Unit separates fluids migrating from deep Mesozoic sources through the lower compartment located below the Blue Unit and microbial hydrocarbons migrating through the upper compartment located above the Blue Unit. Such a system is known as a seal bypass system (Cartwright *et al.* 2007). This fluid flow partition between both compartments is also supported by very low geothermal gradients (Fig. 6) measured at Sites U1324 ($18°C\ km^{-1}$) and U1322 ($26°C\ km^{-1}$) in the upper compartment, despite the presence of sediments with normal to high thermal conductivities (up to $1.4\ W\ mK^{-1}$ measured at both Sites U1322 and U1324, particularly in mass transport deposits.

Furthermore, the few pockmarks at the seafloor, fed by very narrow pipes rising from the Blue Unit (Moore *et al.* 2007), and the large number of mud volcanoes with a deep source suggest a high trapping efficiency of the overpressured Blue Unit across the Mars-Ursa Basin. If this system is widespread, it may explain significant heterogeneities in salinities, thermal regimes and fluid flow evidenced in the northern Gulf of Mexico and the inhibition of gas hydrate formation (Ruppel *et al.* 2005) in the area.

Downward seawater flow evidenced from sulphate profiles

In most marine environments, the oxidation of sedimentary organic matter is mediated by microbial sulphate reduction. However, in anoxic environments dominated by methane advection from depth, anaerobic methane oxidation is likely to be an important process that controls sulphate consumption (Borowski *et al.* 1999). In this case, the sulphate–methane transition zone is positioned at the depth where the concentrations of sulphate and methane reach their minimum (Hensen *et al.* 2003). This correlation is in part due to the rapid consumption of sedimentary organic matter by sulphate reduction and early microbial production of methane during burial (Borowski *et al.* 1999).

In the Mars-Ursa Basin, sulphate profiles are characterized by a high variability in the upper 0–37 mbsf at site U1322 and 0–49 mbsf at site U1324. Below, sulphate decreases rapidly and linearly to the analytical detection limit of 2.89 mM at 74 mbsf (U1322) and 94 mbsf (U1324), thus defining the depth of the sulphate–methane transition zone at both sites. Deep sulphate–methane transition zones have been documented in other basins: 3.5–10 mbsf offshore Namibia (Niewohner *et al.* 1998), 3–6 mbsf along the Chilean continental margin (Treude *et al.* 2005), 6–22 mbsf in the Norwegian Sea (Vuletich *et al.* 1989), 3–13 mbsf on the Nankai Trough (Gamo *et al.* 1993), 35–85 mbsf on the Peru Margin (Biddle *et al.* 2005), 20 mbsf on the Blake Ridge (Borowski *et al.* 2000), 5–54 mbsf in the western Gulf of Mexico (Presley *et al.* 1973) and 3–12 mbsf in the northern Gulf of Mexico (Paull *et al.* 2005). The deepest sulphate–methane transition zone has been found in the Sulu and Celebes Seas at 172 mbsf (Von Breymann *et al.* 1991). The sulphate–methane transition zones measured in the Mars-Ursa Basin is amongst the deepest thus far documented.

Linear sulphate gradients near the base of the sulphate reduction zone are commonly assumed to result from downward diffusive flux of water that is balanced by upward diffusive flux of methane on a steady-state basis, with anaerobic methane oxidation occurring at the base of the sulphate reduction zone (Borowski *et al.* 1999; Treude *et al.* 2005). However, sulphate concentrations exhibit concave-up profiles, with high sulphate concentrations that may be due to sulfide oxidation (Schulz *et al.* 1994), potentially from pyrite minerals as observed in the core analyses (Flemings *et al.* 2005). Such concave-profiles can be interpreted as the result of a re-equilibrium following a mass wasting event (Zabel & Schulz 2001; Hensen *et al.* 2003). In the study area, one mass transport deposit, 15 and 20 m thick at Sites U1324 and U1322 respectively, is positioned above the sulphate–methane transition zone. This single event does not explain the elevated sulphate concentrations in the first 0–37 m and 0–49 mbsf at both drilled sites. As shown in the western Argentine Basin and on the Blake Ridge, such high sulphate gradients can be explained by downward sulphate penetration and diffusive sulphate fluxes into sediments (Dickens 2001; Hensen *et al.* 2003).

As sulphate profiles are sub-linear from 37 mbsf (hole U1322) and 49 mbsf (hole U1324) down to the sulphate–methane transition zone, the flux of sulphate into sediments can be calculated using Fick's First Law (Eqn 1). This law is commonly used for calculating downward sulphate fluxes from pore water sulphate concentrations (Hensen *et al.* 2003).

$$J = D_0 \Phi^3 \frac{\partial C}{\partial x} \quad (1)$$

where J is the flux of sulphate, D_0 is free-solution diffusion coefficient, Φ is porosity, and $\partial C/\partial x$ is the concentration gradient (Lerman 1979).

Given a sulphate diffusion coefficient of 5.8×10^{-6} cm sec^{-1} at 6°C (Li & Gregory 1974), a mean sediment porosity of 55% at Site U1322 and 60% at Site U1324 for the base of the sulphate reduction zone, the sulphate gradients predict sulphate fluxes of 75 and 96×10^{-4} mmol cm^{-2} year^{-1} respectively. This first approximation shows that sulphate fluxes coming from seawater are about 5–10 times higher than those measured in other basins, such as 8 to 18×10^{-4} mmol cm^{-2} year^{-1} on the Blake Ridge (Borowski *et al.* 2000).

The fluid flow rate (and thus methane flux) is almost constant with depth at each site, reflecting a constant lateral and vertical overpressure gradient in sediments overlying the Blue Unit. Therefore, the depth of the sulphate–methane transition zone is driven by the rate of the downward sulphate-rich seawater flux, instead of a variation of the upward methane flux (Fig. 6).

Possible causes for downward seawater flow

The large number of palaeo-mud volcanoes identified on seismic data suggests that mud and fluid expulsion has been active in this area for a prolonged period of time. The fact that mud volcanoes become extinct also suggests variability in the overall rate and locus of mud expulsion to the seabed. A possible explanation is that this mud volcanism is driven by the basinward progradation leading to a loading of underlying sediments and a continuous pressure build-up within a deep seated reservoir, which episodically releases the overpressure (Kopf 2002).

The presence of large mud volcanoes close to the drilled sites may disturb fluid flow in shallow sediments (Henry *et al.* 1996). Mud volcanoes and seafloor piercing structures represent effective pathways of fluid migration from the deep subsurface to the seabed (Kopf 2002; Sassen *et al.* 2003b). Mud and fluid flow rates from these features can be high enough to locally increase the heat flow regime by rapidly transferring warmer fluids from the deep subsurface to the seafloor (Eldholm *et al.* 1999; Grevemeyer *et al.* 2004; Kaul *et al.* 2006). Furthermore, fluids are generally expelled through a zone much larger than the mud volcano itself due to lateral diffusion (Henry *et al.* 1996). The combination between upward warm fluid migration, wide area of fluid migration around the mud volcanoes, and the density difference of released fluids with seawater will induce downwelling of seawater away from the mud volcanoes and flow towards the mud volcanoes at depth.

Recent studies have shown that the fluid flow pattern can also be explained by geothermal convection of seawater in any setting with a sloping seafloor (Phillips 1991; Sanford *et al.* 1999). Geothermal convection of seawater has been documented in the Floridian Plateau (Kohout 1967), in coral reef environments (Rougerie & Wauthy 1993), or on mid-Pacific guyots (Paull *et al.* 1995). The mechanism involved is a temperature difference between the warm interiors of shelves/slopes and cold seawaters leading to a natural buoyancy-driven flow system. This geothermal convection is also known as the endo-welling concept (Rougerie & Wauthy 1993; Tribble *et al.* 1994; Keating & Helsley 2000) which has to be taken into account for shallow (<1000 m) processes and in particular slope instabilities (Keating & McGuire 2000). Recent numerical modelling has shown that this geothermal convection of seawater appears confined largely to the uppermost 2 km of sediments (Wilson 2003). Such convective cells may drive downward sulphate-rich seawater flow and explain the high sulphate gradients observed in the first tens of metres below the seafloor. Similar process has been evidenced in the Blake-Bahama Platform where strontium analyses indicate flushing by modern seawater to depths up to 400 m below the seafloor (Ussler *et al.* 2000). Furthermore, the calculated downward sulphate flux is greater in U1324, which is closer to the wide mud volcano and might be more influenced by variations in geothermal gradient.

CONCLUSIONS

Based on geophysical and geochemical signature of a fluid flow system over an overpressured sand-rich interval in the Mars-Ursa Basin, Gulf of Mexico, we have shown that:

(1) The sulphate–methane transition zones measured at Mars-Ursa Basin are 94 m at Site U1324 and 74 m at Site U1322, which is amongst the deepest ever found in deep sedimentary basins.
(2) Sulphate profiles suggest diffuse downward seawater flow in the first tens of metres below the seafloor.
(3) The downward seawater flow is consistent with the calculated downward sulphate fluxes into sediments that are about 5–10 times higher than those measured in other basins.
(4) The depth of the sulphate–methane transition zone is driven by the combination of a downward flow of sulphate-rich seawater and a low upward methane flux.

(5) The lateral basinward fluid flow in an overpressured interval can separate sedimentary compartments below and above. Overpressure in the lower compartment leads to episodic and focused fluid migration through deep conduits that bypass the upper compartment, forming mud volcanoes at the seabed.
(6) Methane can bypass the shallow subsurface where most of the geochemical reactions occur in order to reduce methane concentration. This might explain the absence of gas hydrate layer in this prolific hydrocarbon province. This has also important implications for climate studies as methane can vent directly to the water column.

These conclusions show that shallow physical and chemical processes impact surface seepage and have to be considered when interpreting underlying overpressured aquifers and reservoirs. In particular, the separation between the different compartments allows for unexpected pore pressure profiles in the overlying sediments. Piercing structures, namely pockmarks and mud volcanoes, may induce a geothermal convection, also known as the endo-welling concept, possibly leading to a downward flow of seawater into shallow sediments. These processes have to be taken into account for drilling operations and when assessing the stability of submarine slopes.

ACKNOWLEDGEMENTS

This work was partly supported by IODP France and collaborative French universities, in particular Géosciences Montpellier at University of Montpellier 2. We are very grateful to technicians and crew of the JOIDES-Resolution who provided a great help and support during the cruise. We also would like to thank SHELL for providing us with 3D seismic data of high quality and resolution, and a special thank to Carlos Pirmez who always supported this work.

This research was also partly supported by a Grant-In-Aid (No. 18004043) from the Japan Society for the Promotion of Science (JSPS) and a 21st Century Center of Excellence (COE) Program on 'Neo-Science of Natural History' at Hokkaido University financed by the MEXT (Ministry of Education, Culture, Sports, Science and Technology) of Japan.

We would like to thank Mads Huuse, Lieven Naudts and an anonymous reviewer for their constructive suggestions on the manuscript. Their comments were appreciated as they forced us to ask more and more questions. They also gave us keys to not be lost in combining results from different sources.

REFERENCES

Behrmann J, Flemings P, John C, Scientists TE3 (2006) Rapid sedimentation, overpressure and focused fluid flow, Gulf of Mexico continental margin. *Scientific Drilling*, **3**, 12–17.

Berndt C (2005) Focused fluid flow in passive continental margins. *Philosophical Transactions of the Royal Society A: Mathematical, Physical and Engineering Sciences*, **363**, 2855–71.

Biddle J, House C, Brenchley J (2005) Microbial stratification in deeply buried marine sediment reflects changes in sulphate/methane profiles. *Geobiology*, **3**, 287–95.

Borowski W, Paull C, Ussler W III (1999) Global and local variations of interstitial sulphate gradients in deep-water, continental margin sediments: sensitivity to underlying methane and gas hydrates. *Marine Geology*, **159**, 131–54.

Borowski W, Hoehler T, Alperin M, Rodriguez N, Paull C (2000) Significance of anaerobic methane oxidation in methane-rich sediments overlying the Blake Ridge gas hydrates. In: *Proceedings of the Ocean Drilling Program, Scientific Results* (eds Paull C, Matsumoto R, Wallace P, Dillon W), **Vol. 164**, pp. 87–99. Texas A&M University, College Station, TX.

Brooks J, Kennicutt M, Fay R, McDonald T (1984) Thermogenic gas hydrates in the Gulf of Mexico. *Science*, **225**, 409–11.

Cartwright J, Huuse M, Aplin A (2007) Seal bypass system. *AAPG Bulletin*, **91**, 1141–66.

Cathles L (2004) Hydrocarbon generation, migration, and venting in a portion of the offshore Louisiana Gulf of Mexico basin. *The Leading Edge*, **23**, 760–65.

Coleman J, Roberts H (1988) Sedimentary development of the Louisiana continental shelf related to sea level cycles: Part II: seismic response. *Geo-Marine Letters*, **8**, 109–19.

Cosgrove J, Hillier R (2000) Forced-fold development within Tertiary sediments of the Alba Field, UKCS; evidence of differential compaction and post-depositional sandstone remobilization. In: *Forced Folds and Fractures* (eds Cosgrove J, Ameen M), **Vol. 169**, pp. 61–71. Geological Society of London Special Publication, London.

Davies R, Stewart S (2005) Emplacement of giant mud volcanoes in the South Caspian Basin: 3D seismic reflection imaging of their root zones. *Journal of the Geological Society*, **162**, 1–4.

Dickens G (2001) Sulphate profiles and barium fronts in sediment on the Blake Ridge: present and past methane fluxes through a large gas hydrate reservoir. *Geochimica et Cosmochimica Acta*, **65**, 529–43.

Dugan B, Flemings P (2002) Overpressure and fluid flow in the New Jersey continental slope: implications for the slope failure and cold seeps. *Science*, **289**, 288–91.

Eldholm O, Sundvor E, Vogt P, Hjelstuen B, Crane K, Nilsen A, Gladczenko T (1999) SW Barents Sea continental margin heat flow and HÃ¥kon Mosby Mud Volcano. *Geo-Marine Letters*, **19**, 29–37.

Flemings P, Behrmann J, John C and the Expedition 308 Scientists' (2005) *Gulf of Mexico Hydrogeology*, Proceedings of the Integrated Ocean Drilling Program, 308, Texas A&M University, College Station, TX.

Fu B, Aharon P (1998) Sources of hydrocarbon-rich fluids advecting on the seafloor in the northern Gulf of Mexico. *AAPG Bulletin*, **82**, 1781.

Gamo T, Kastner M, Berner U, Gieskes J (1993) Carbon isotope ratio of total inorganic carbon in pore waters associated with diagenesis of organic material at Site 808, NankaiTrough. In: *Proceedings of Ocean Drilling Program, Scientific Results* (eds Hill I, Taira A, Firth J), **Vol. 131**, pp. 159–63. Texas A&M University, College Station, TX.

Gay A, Lopez M, Berndt C, Séranne M (2007) Geological controls on focused fluid flow associated with seafloor seeps in the Lower Congo Basin. *Marine Geology*, **244**, 68–92.

Gay A, Lopez M, Cochonat P, Levaché D, Sermondadaz G, Séranne M (2006) Evidences of early to late fluid migration

from an Upper Miocene turbiditic channel revealed by 3D seismic coupled to geochemical sampling within seafloor pockmarks. *Lower Congo Basin, Marine and Petroleum Geology*, **23**, 387–99.

Gieskes J, Gamo T, Brumsack H (1991) Chemical methods for interstitial water analysis aboard Joides Resolution. *Ocean Drilling Program Technical Note*, **15**, 60.

Grevemeyer I, Kopf A, Fekete N, Kaul N, Villinger H, Heesemann M, Wallmann K, Spiess V, Gennerich H, Müller M, Weinrebe W (2004) Fluid flow through active mud dome Mound Culebra offshore Nicoya Peninsula, Costa Rica: evidence from heat flow surveying. *Marine Geology*, **207**, 145–57.

Henry P, Le Pichon X, Lallemant S, Lance S, Martin J, Foucher J, Medioni F, Rostek F, Guilhumou N, Pranal C, Castec M (1996) Fluid flow in and around a mud volcano field seaward of the Barbados accretionary wedge: results from Manon cruise. *Journal of Geophysical Research*, **101**, 20297–323.

Hensen C, Zabel M, Pfeifer K, Schwenk T, Kasten S, Riedinger N, Schulz H, Boetius A (2003) Control of sulphate porewater profiles by sedimentary events and the significance of anaerobic oxidation of methane for the burial of sulfur in marine sediments. *Geochimica et Cosmochimica Acta*, **67**, 2631–47.

Kaul N, Foucher J, Heesemann M (2006) Estimating mud expulsion rates from temperature measurements on Häkon Mosby Mud Volcano, SW Barents Sea. *Marine Geology*, **229**, 1–14.

Keating B, Helsley C (2000) Sonar Studies of Submarine Mass Wasting and Volcanic structures off Savaii Island, Samoa. *Pure and Applied Geophysics*, **157**, 1285–313.

Keating B, McGuire W (2000) Island edifice failures and associated tsunami hazards. *Pure and Applied Geophysics*, **157**, 899–955.

Kohout F (1967) Ground-water flow and the geothermal regime of the Floridian Plateau. *Transactions Gulf Coast Association of Geological Societies*, **17**, 339–54.

Kopf A (2002) Significance of mud volcanism. *Reviews of Geophysics*, **40**, 1–52.

Lerman A (1979) *Geochemical Processes: Water and Sediment Environments*, John Wiley and Sons, New York.

Li Y, Gregory S (1974) Diffusion of ions in sea water and in deep-sea sediments. *Geochimica et Cosmochimica Acta*, **38**, 703–14.

Loncke L, Mascle J, Party FS (2004) Mud volcanoes, gas chimneys, pockmarks and mounds in the Nile deep-sea fan (Eastern Mediterranean): geophysical evidences. *Marine and Petroleum Geology*, **21**, 669–89.

Løseth H, Wensaas L, Arntsen B, Hanken N, Basire C, Graue K (2001) 1000 m long gas blow out pipes. 63rd EAGE Conference and Exhibition, Extended Abstracts, 524.

MacDonald I, Guinasso N Jr, Ackleson S, Amos J, Duckworth R, Sassen R, Brooks J (1993) Natural oil slicks in the Gulf of Mexico visible from space. *Journal of Geophysical Research*, **98**, 16351–64.

MacDonald I, Leifer I, Sassen R, Stine P, Mitchell R, Guinasso N Jr (2002) Transfert of hydrocarbons from natural seeps to the water column and atmosphere. *Geofluids*, **2**, 95–107.

McAdoo B, Pratson L, Orange D (2000) Submarine landslide geomorphology, US continental slope. *Marine Geology*, **169**, 103–36.

McFarlan E, LeRoy D (1988) Subsurface geology of the late Tertiary and Quaternary deposits, coastal Louisiana, and the adjacent continental shelf. *Gulf Coast Association of Geological Societies Transactions*, **38**, 421–33.

Milkov A, Sassen R (2000) Thickness of the gas hydrate stability zone, Gulf of Mexico continental slope. *Marine and Petroleum Geology*, **17**, 981–91.

Moore J, Iturrino G, Flemings P, Hull I, Gay A (2007) Fluid migration and state of stress above the Blue Unit, Ursa Basin: relationship to the geometry of injectites. *OTC*, **18812**.

Moss J, Cartwright J (in press) 3D seismic expression of Km-scale fluid escape pipes from offshore Namibia. *Basin Research*.

Niewohner C, Henson C, Kasten S, Zabel M, Schultz H (1998) Deep sulphate reduction completely mediated by anaerobic methane oxidation in sediments of the upwelling area off Namibia. *Geochimica et Cosmochimica Acta*, **62**, 455–64.

Osborne M, Swarbrick R (1997) Mechanisms for generating overpressure in sedimentary basins; a reevaluation. *AAPG Bulletin*, **81**, 1023–41.

Paull C, Fullgar P, Bralower T, Rohl U (1995) Seawater ventilation of mid-Pacific guyots drilled during Leg 143. *Proceedings of Ocean Drilling Program Scientific Results*, **143**, 231–41.

Paull C, Ussler W III, Lorenson T, Winters W, Dougherty J (2005) Geochemical constraints on the distribution of gas hydrates in the Gulf of Mexico. *Geo-Marine Letters*, **25**, 273–80.

Phillips O (1991) *Flow and Reactions in Permeable Rocks*, Cambridge University Press, New York.

Pimmel A, Claypool G (2001) Introduction to Shipboard organic geochemistry on the JOIDES Resolution. *Ocean Drilling Program Technical Note*, **30**, 29.

Presley B, Petrowski C, Kaplan I (1973) Interstitial water chemistry. In: *Initial Reports of Deep Sea Drilling Project* (eds Worzel J, Bryant W), **Vol. 10**, pp. 613–14. U.S. Government Printing Office, Washington.

Pulham A (1993) Variations in slope deposition, Pliocene-Pleistocene, offshore Louisiana, northeast Gulf of Mexico. In: *Siliclastic Sequence Stratigraphy: Recent Developments and Applications* (eds Posamentier H, Weimer P), **Vol. 58**, pp. 199–233. AAPG Memoir, Mobile, USA.

Rougerie F, Wauthy B (1993) The endo-upwelling concept: from geothermal convection to reef construction. *Coral Reefs*, **12**, 19–30.

Ruppel C, Dickens G, Castellini D, Gilhooly W, Lizarralde D (2005) Heat and salt inhibition of gas hydrate formation in the northern Gulf of Mexico. *Geophysical Research Letters*, **32**, 1–4.

Sanford W, Whitaker F, Smart P, Jones G (1999) Numerical analysis of seawater circulation in carbonate platforms: geothermal convection. *American Journal of Science*, **298**, 801–28.

Sassen R, Cole D, Drozd R, Roberts H (1994) Oligocene to Holocene hydrocarbon migration and salt-dome carbonates, northern Gulf of Mexico. *Marine and Petroleum Geology*, **11**, 55–65.

Sassen R, Joye S, Sweet S, DeFreitas D, Milkov A, MacDonald IR (1999) Thermogenic gas hydrates and hydrocarbon gases in complex chemosynthetic communities, Gulf of Mexico continental slope. *Organic Geochemistry*, **30**, 485–97.

Sassen R, Milkov A, Ozgul E, Roberts H, Hunt J, Beeunas M, Chanton J, DeFreitas D, Sweet S (2003a) Gas venting and subsurface charge in the Green Canyon area, Gulf of Mexico continental slope: evidence of a deep bacterial methane source? *Organic Geochemistry*, **34**, 1455–64.

Sassen R, Milkov A, Roberts H, Sweet S, DeFreitas D (2003b) Geochemical evidence of rapid hydrocarbon venting from a seafloor-piercing mud diapir, Gulf of Mexico continental shelf. *Marine Geology*, **198**, 319–29.

Sawyer D, Flemings P, Shipp R, Winker C (2007) Seismic geomorphology, lithology, and evolution of the late pleistocene Mars-Ursa turbidite region, Mississippi canyon area, northern Gulf of Mexico. *AAPG Bulletin*, **91**, 215–34.

Schulz H, Dahmke A, Schinzel U, Wallmann K, Zabel M (1994) Early diagenesis processes, fluxes, and reaction rates in sediments of the South Atlantic. *Geochimica et Cosmochimica Acta*, **58**, 2041–60.

Stewart S, Davies R (2006) Structure and emplacement of mud volcano systems in the South Caspian Basin. *AAPG Bulletin*, **90**, 771–86.

Treude T, Niggemann J, Kallmeyer J, Wintersteller P, Schubert C, Boetius A, Jorgensen B (2005) Anaerobic oxidation of methane and sulphate reduction along the Chilean continental margin. *Geochimica et Cosmochimica Acta*, **69**, 2767–79.

Tribble G, Atkinson J, Sansone F, Smith S (1994) Reef metabolism and endo-upwelling in perspective. *Coral Reef*, **13**, 199–201.

Tsunogai U, Yoshida N, Gamo T (1999) Carbon isotopic compositions of C2-C5 hydrocarbons and methyl chloride in urban, coastal and maritime atmosphere over western-North Pacific. *Journal of Geophysical Research*, **104**, 16033–9.

Urgeles R, Locat J, Flemings P, Behrmann J, John C, Expedition 308 shipboard scientific party (2007) Mechanisms leading to overpressure and slope instability in the Gulf of Mexico continental slope. In: *Geophysical Research Abstracts* (ed. European Geoscience Union). EGU, Vienna, Austria, 9, A-00457.

Ussler W, Paull C, Fullagar P (2000) Pore-water strontium isotopes from the Leg 171B drilling transect down the Blake Spur. In: *Proceedings of the Ocean Drilling Program Scientific Results* (eds Kroon D, Norris D). Texas A&M University, College Station, TX, 171B, online.

Van Rensbergen P, Morley C, Ang D, Hoan T, Lam N (1999) Structural evolution of shale diapirs from reactive rise to mud volcanism: 3D seismic data from the Baram delta, offshore Brunei Darussalam. *Journal of the Geological Society of London*, **156**, 633–50.

Von Breymann M, Swart P, Brass G, Berner U(1991) Pore water chemistry of the Sulu and Celebes Seas: extensive diagenetic reactions at Sites 767 and 768. In: *Proceedings of the Ocean Drilling Program, Scientific Results* (eds Silver E, Rangin C, von Breymann M), **Vol. 124**, pp. 203–15. Texas A&M University, College Station, TX.

Vuletich A, Threlkeld C, Claypool G (1989) Isotopic composition of gases and interstitial fluids in sediments of the VÃ¸ring Plateau, ODP Leg 104, Site 644. In: *Proceedings of the Ocean Drilling Program, Scientific Results* (eds Eldholm O, Thiede J, Taylor E *et al.*), **Vol. 104**, pp. 281–3. Texas A&M University, College Station, TX, doi: 10.2973/odp.proc.sr.104.199.1989.

Whiticar M (1999) Carbon and hydrogen isotope systematics of bacterial formation and oxidation of methane. *Chemical Geology*, **161**, 291–314.

Wilson A (2003) The occurence and chemical implications of geothermal convection of seawater in continental shelves. *Geophysical Research Letters*, **30**, 1–4.

Winker C, Booth J (2000) Sedimentary dynamics of the salt-dominated continental slope, Gulf of Mexico: integration of observations from the seafloor, near-surface, and deep subsurface. In: 20th Annual Research Conference (ed. GCSSEPM), **20**, 1059–86.

Winker C, Shipp R (2002) Sequence stratigraphic framework for prediction of shallow water flow in the greater Mars-Ursa area, Mississippi Canyon area, Gulf of Mexico continental slope. In: *Sequence Stratigraphic Models for Exploration and Production: Evolving Methodology, Emerging Models, and Application Histories* (ed. Armentrout J). SEPM Gulf Coast Section 22nd Annual Research Conference, Houston, online.

Yu Z, Lerche I (1996) Modelling abnormal pressure development in sandstone/shale basins. *Marine and Petroleum Geology*, **13**, 179–93.

Zabel M, Schulz H (2001) Importance of submarine landslides for non-steady state conditions in pore water systems – Lower Zaire (Congo) deep-sea fan. *Marine Geology*, **176**, 87–99.

Zitter T, Huguen C, Woodside J (2005) Geology of mud volcanoes in the eastern Mediterranean from combined sidescan sonar and submersible surveys. *Deep-Sea Research I*, **52**, 457–75.